(Received 30 December 2025, Accepted 4 February 2026, Scheduled 6 March 2026)

AC Losses Modeling in ReBCO Superconducting Coils Using the Volume Integral Method

Sara Fawaz[1] and Hocine Menana[2,*]

[1] ESME, ESME Research Lab, Campus de Lille, F-59000 Lille, France
[2] Université de Lorraine, GREEN, F-54000 Nancy, France

ABSTRACT: This paper presents a fast and efficient modeling approach based on the volume integral method for the characterization of AC losses in high-temperature superconducting coils made of second-generation Rare-earth Barium Copper Oxide (ReBCO) tapes. Three modeling strategies are investigated and compared, considering the detailed multilayer tape configuration, the homogenized tape configuration, and the simplified single-layer superconducting tape representation. These approaches aim to evaluate the impact of geometrical and electromagnetic simplifications on the accuracy of the results while significantly reducing computational time. In particular, the homogenization of the electromagnetic properties of the tape is explored to accelerate simulations without compromising the accuracy of key physical quantities, such as AC losses and current density distribution. The modeling results are compared to measurements.

1. INTRODUCTION

High temperature superconductors (HTSs) hold significant potential for applications in electrical power systems, such as electrical machines, energy storage systems, and superconducting fault current limiters [1–3]. Their main advantage lies in their ability to conduct high current densities with minimal energy loss at relatively low cryogenic costs.

However, despite their negligible DC losses, HTSs are subject to significant losses when carrying alternating currents (AC) or exposed to time-varying magnetic fields. These losses represent a major limitation for practical use, as they directly affect the efficiency of HTS-based systems. Accurate evaluation of AC losses is thus essential to properly size and ensure the reliable operation of HTS systems [4, 5].

Traditional analytical approaches based on the critical state model allow a first estimation of AC losses, but they generally neglect the dependence of the critical current density on the magnetic field [6, 7]. As a result, they are limited to simplified geometries that do not reflect the complexity of real HTS systems [8]. To overcome these limitations, numerical methods using the power-law have been widely adopted, offering a more accurate representation of the nonlinear electromagnetic behavior of HTS [9–11]. Nevertheless, such methods can become computationally expensive, particularly when being applied to complex, multi-scale structures, such as HTS coils.

To achieve a balance between accuracy and computational cost, semi-analytical methods based on volume integral equations have been developed [12–14]. These approaches offer a good compromise by limiting the discretization to the active regions of the modeled systems.

Given the structural complexity of HTS systems, including heterogeneities, anisotropies, and multi-scale geometries, combined with the strong nonlinearity of their electromagnetic properties, modeling becomes both a critical and resource-intensive task. As a result, dedicated strategies are required for the efficient simulation and design of superconducting systems.

In this context, the present work investigates, within a two-dimensional framework, three strategies for modeling AC losses in HTS coils made of Rare-earth Barium Copper Oxide (ReBCO) tapes which are compared, with a particular focus on the homogenization applied at the tape level. The volume integral method is employed, allowing for discretization to be limited to the conducting and superconducting domains. The modeling results are then compared to measurements to assess the accuracy of the proposed modeling strategies.

The modeling approach is detailed in the next section, followed by the presentation and discussion of numerical and experimental results in Section 3.

2. MODELING APPROACH

The modeled system consists of a single-layer pancake inductive coil of inner and outer radii denoted as R_{int} and R_{ext}, respectively. The coil is composed of N_t turns of ReBCO tape as shown in Fig. 1, where H_t and W_t represent the width and thickness of the tape. Such tape has a multilayer structure, where the superconducting layer thickness is about 2 µm [15].

The modeling strategies consider three tape configurations. The first is a multilayer tape configuration, which explicitly represents the main tape layers (Copper, Re-BCO, and Hastelloy). The second is a homogenized tape configuration, where the tape is treated as a single, uniform superconducting entity. The third is a single-layer superconducting tape configuration, which focuses solely on the superconducting (Re-BCO) layer of 2 µm. In the multilayer tape model, the resistivity values of

* Corresponding author: Hocine Menana (hocine.menana@univ-lorraine.fr).

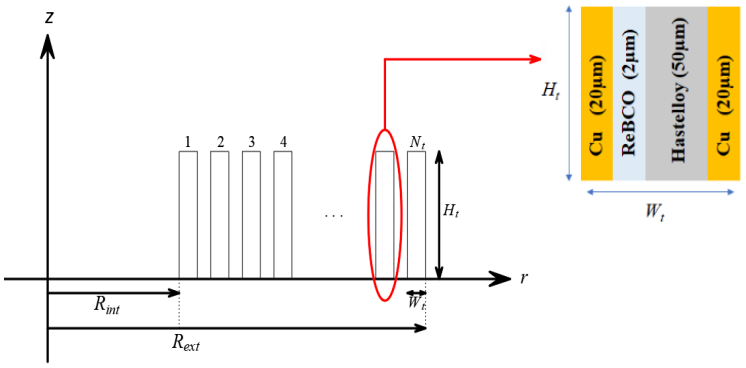

FIGURE 1. Modeled system with a schematic layout of the considered multilayer structure of the REBCO tapes.

TABLE 1. Parameters specification.

Parameter	Value	Description
W_t/H_t	0.092/4 mm	Tape thickness/Tape width
R_{ext}/R_{int}	6.2/6 cm	External/Internal radius of the coil
N_t	6	Number of the coil turns
$\rho_{Cu(77K)}$	$0.19 \times 10^{-8}\,\Omega \cdot$ m	Electrical resistivity of Copper at 77 K
$\rho_{Hast(77K)}$	$124 \times 10^{-8}\,\Omega \cdot$ m	Electrical resistivity of Hastelloy at 77 K
E_c	1 µV/cm	Critical electric field
n	18/30	Creep exponent for the multilayer/homogenized and superconducting layer tape model
I_{c0}	140 A	Critical current at zero magnetic field
k	0.15	Parameter of anisotropy used in (1)
B_0/β	0.14 T/1.39	Kim's parameters used in (1)
γ	100 V/(A·m)	Feedback constant

Copper and Hastelloy at cryogenic temperatures are used [16] and provided in Table 1.

The electric resistivity of the superconducting region is nonlinear and modeled by a power law relation, associated with Kim's law [16] describing the dependence of the critical current density on the magnetic field. Both relations are given in (1). In this expression, E and E_c represent the electric field and its critical value; J and J_c are the electric current density and its critical value; n is the creep exponent characterizing the steepness of the transition from the superconducting to normal state; J_{c0} is the electric current density at zero magnetic field; B_r and B_z are respectively the components of the magnetic field in the radial and axial directions; and B_0, k, and β are parameters depending on the material. The superconducting and normal regions are denoted respectively by Ω_s and Ω_n. All regions of the system are characterized by the vacuum magnetic permeability μ_0.

$$\begin{cases} \vec{E} = E_c \left(J_c(B)\right)^{-n} J^{n-1} \vec{J} \\ J_c(B) = J_{c0} \left(1 + B_0^{-1} \sqrt{k^2 B_z^2 + B_r^2}\right)^{-\beta} \end{cases} \tag{1}$$

The modeling approach is based on the expression of the electric field as a function of the magnetic vector and electric scalar potentials $(\vec{A}, V)$ as follows:

$$\vec{E} = -\partial_t \vec{A} - \vec{\nabla} V \tag{2}$$

Given the symmetry of revolution of the coil, a 2D axisymmetric modeling approach is considered. The term $\vec{\nabla} V$ is, in this case, truncated by an integral ensuring the current conservation as given in (3), where S_t is the cross-sectional area of the tape, and I_a is the applied current.

$$\iint_{S_t} J ds = I_a \tag{3}$$

Expressing the magnetic vector potential $\vec{A}$ in its integral form as a function of the electric current density in (2), and incorporating the current conservation constraint from Equation (3), yields the following equation:

$$E_{(\vec{p})} + \sum_{Nt} \iint_{S_t} G_{(\vec{p},\vec{q})} \partial_t J_{(\vec{q})} ds + \gamma \iint_{S_t \ni \vec{p}} (J - J_a)\, ds = 0 \tag{4}$$

where $G_{(\vec{p},\vec{q})}$ is the Green's function expressed in terms of the position vectors $\vec{p}$ and $\vec{q}$, locating the calculation point and the source point, respectively; J_a is the applied current density assumed uniform; and γ is a feedback constant [17]. In (4), it is

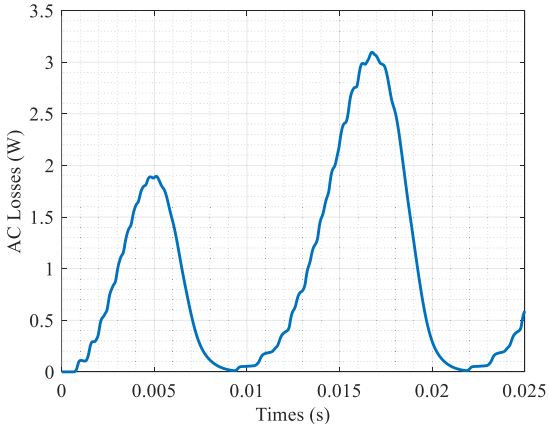

FIGURE 2. Instantaneous AC losses for the HTS coil over one period computed for the multilayer tape configuration ($I_{\max} = 110\,\text{A}$, $f = 40\,\text{Hz}$).

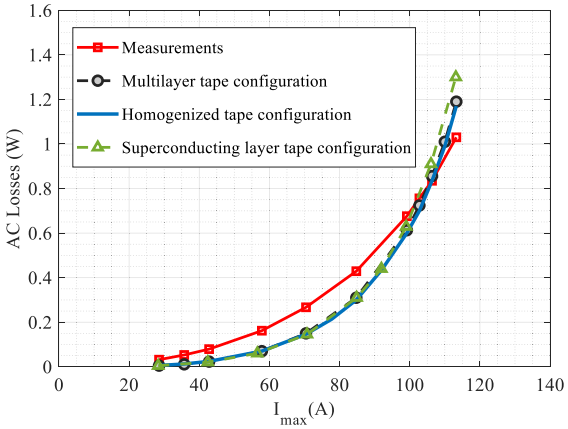

FIGURE 3. Comparison between experimental measurements and numerical results of AC losses obtained for the different tape configurations ($f = 40\,\text{Hz}$).

assumed that all the points contained in a tape cross-section are at the same electric potential.

The AC losses are then evaluated as follows:

$$P = 2\pi \sum_{Nt} \iint_{S_t} r_{(\vec{p})} E_{(\vec{p})} J_{(\vec{p})} ds \tag{5}$$

Each tape section is discretized into $N_r \times N_z$ rectangular elements of surface ΔS along the radial and axial directions, respectively. Introducing (1) in (4), the matrix form of the resulting equation is given as follows:

$$\bar{\bar{G}}\partial_t \bar{J} + \bar{\bar{\delta}}_s E_c \left[\bar{J}/\bar{J}_c\right]^n + \left(1 - \bar{\bar{\delta}}_s\right)\bar{\bar{\rho}}\bar{J} + \gamma \bar{\bar{S}}_t \left\{\bar{J} - \bar{J}_a\right\} = \vec{0} \tag{6}$$

The matrix $\bar{\bar{\rho}}$, which is diagonal, represents the resistivity of the normal regions, and the matrix $\bar{\bar{\delta}}_s$, which is also diagonal, is introduced to distinguish between the superconductive and normal regions: $\bar{\bar{\delta}}_{s(i,i)} = \{1 \text{ if } i \in \Omega_s,\ 0 \text{ if } i \in \Omega_n\}$. The matrix system (6) is highly nonlinear. It is solved using the "ode15s" solver in Matlab [18].

3. RESULTS AND DISCUSSIONS

The studied HTS coil has been characterized experimentally using the electric method at the liquid nitrogen temperature [19]. Details on the experimental characterization are provided in the appendix. The parameter specifications of the modeled system are given in Table 1.

This section provides the numerical results of the current density J distribution in the coil cross-section, obtained by solving Equation (6), under the application of a sinusoidal current defined as $I_a = I_{\max} \sin(2\pi f t)$. The corresponding AC losses are calculated using Equation (5) and compared to experimental measurements.

The homogenized tape configuration simply assumes that the whole tape section is superconducting. The critical current density is thus defined for the tape section ($J_c = I_c/S_t$), while the critical current I_c is the same in the three configurations.

Each tape constituting the coil is discretized into $N_z = 30$ elements in the z direction. The discretization in the radial direction depends on the configuration used: $N_r = 20$ for the multilayer tape configuration, $N_r = 6$ for the homogenized tape configuration, and $N_r = 1$ for the single superconducting layer configuration. The selected discretization values were found to provide a good compromise between result accuracy and time consumption, as increasing the number of elements led to only negligible variations in the results.

For the multilayer tape configuration, $N_r = 20$ was adopted, corresponding to a detailed discretization of the different material layers: the 2 µm REBCO layer discretized into 2 elements, the two 20 µm copper layers discretized into 4 elements each, and the 50 µm Hastelloy layer discretized into 10 elements. Finer discretization did not significantly improve the results.

For the homogenized tape configuration, a radial discretization of $N_r = 6$ was chosen by considering an equivalent homogenized tape thickness of 92 µm. Higher values of N_r were tested and showed no noticeable impact on the results.

Finally, for the single superconducting layer configuration, $N_r = 1$ was considered sufficient due to the small thickness of the REBCO layer (2 µm).

In all configurations, the axial discretization was fixed to $N_z = 30$, which was found to ensure stable and accurate results.

The instantaneous AC losses for a sinusoidal applied current of 110 A amplitude and 40 Hz frequency are reported in Fig. 2, computed for the multilayer tape configuration. The steady state regime is obtained in the second half period. The average AC losses are then obtained by averaging the instantaneous losses on the second half of the period. A similar evolution is obtained for all the tape configurations.

The AC losses obtained for the three tape configurations are compared to measurements for different applied currents at a frequency of 40 Hz. As shown in Fig. 3, the three tape configurations lead to very close results, highlighting the possibility of tape homogenization, or that of simply neglecting the normal regions. This also means that the hysteresis losses in the HTS part are predominant at low frequencies. The difference with

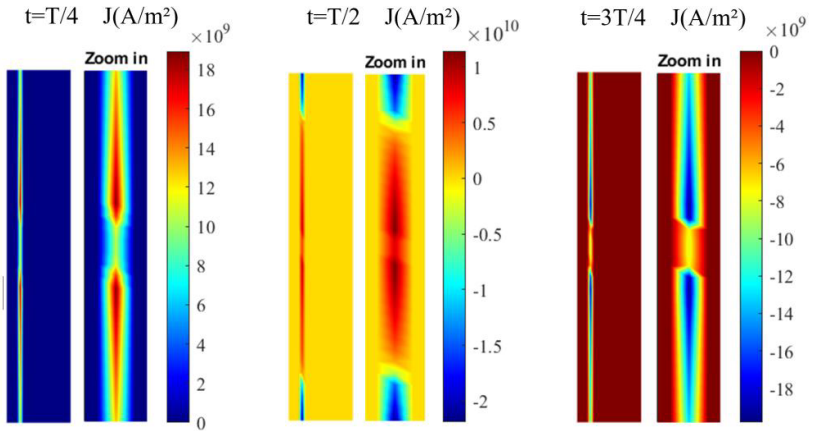

FIGURE 4. Distribution of the electric current density in a tape for the multilayer tape configuration at three different instants: $T/4, T/2$ and $3T/4$, where T is the period ($I_{\text{max}} = 110$ A, $f = 40$ Hz). The figures are zoomed in on the superconducting layer and are not drawn to scale.

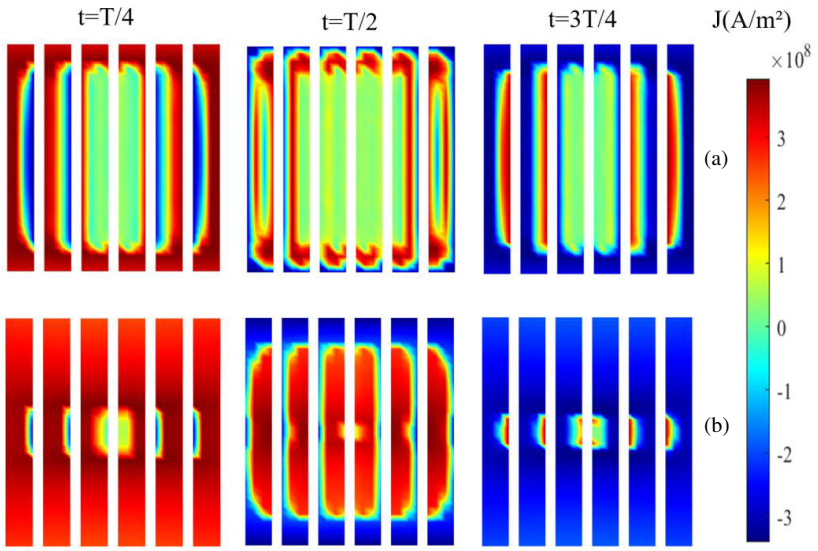

FIGURE 5. Distribution of the electric current density in the HTS coil cross-section for the homogenized tapes configuration, at different instants over one AC cycle, at a frequency $f = 40$ Hz for two applied currents: (a) $I_{\text{max}} = 50$ A and (b) $I_{\text{max}} = 110$ A.

the measurements may be due to uncertainties in the Kim's parameters used in (1), which are obtained for applied magnetic fields, while the coil is in the self-field [20].

Figure 4 illustrates the distribution of J in a tape at different instants expressed as a function of the period T of the waveform, for the multilayer tape configuration for an applied current amplitude $I_{\text{max}} = 110$ A, at a frequency $f = 40$ Hz. Notice that the figures are not to scale zooming on the superconducting layer. As we can notice, the current predominantly flows through the superconducting region rather than the normal conducting region, since the applied current remains below the coil's critical current. As the current decreases, a reverse current is induced starting from the outer surface of the superconducting layer in order to minimize the magnetic energy. This results in two opposing currents of equal amplitude within each tape section, with current densities depending on the strength of the local magnetic flux density, when the applied current is nil ($I_a = 0$). This phenomenon maintains a certain magnetic energy in the tapes not returned to the source, which is the origin of the hysteresis losses. The current density repartition is the same in all the tapes. The computation time is about 45 minutes, once the matrices have been calculated.

Figure 5 presents the distribution of J for the homogenized configuration for two values of the applied current ($f = 40$ Hz). Similar to the multilayer case, the current penetrates each tape from the outer surface to a depth determined by the applied current and the critical current density, which varies with the magnetic flux density, in particular, its radial component (B_r). Higher penetration is observed on tapes located at the ends of the coil, which are exposed to high magnetic flux densities at the corners.

For the same applied current, compared to the multilayer tape configuration, the computation time is reduced by a factor of 20, considering the homogenized configuration, and by a factor of 1300, considering the single-layer superconducting tape configuration, due to the reduced discretization in the radial direction in this case ($N_r = 1$).

4. CONCLUSIONS

This work presents a fast and efficient modeling approach based on the volume integral method, which restricts discretization to the active parts of the system. This method enables accurate evaluation of electromagnetic quantities, such as current density and AC losses in HTS coils. Three modeling strategies: multilayer, homogenized, and single-layer configurations, were investigated to assess the trade-off between computational cost and accuracy.

The modeling results obtained with each strategy show good agreement with experimental measurements, confirming the validity of the proposed simplifications. In particular, the study demonstrates that homogenizing the superconducting layer at the tape level significantly reduces computation time without compromising accuracy. These results validate the reliability and efficiency of the proposed modeling strategies, making them suitable for the design and optimization of HTS systems. However, with the increase in frequency, it is expected that the eddy current losses in the normal regions will be in the same range as the hysteresis losses in the HTS. In this case, the homogenization of the tapes needs to consider the conductivities of the normal regions.

APPENDIX A. DETAILS ON THE EXPERIMENTAL CHARACTERIZATION

An insulated inductive pancake HTS coil wound with a REBCO tape has been constructed and characterized experimentally. Fig. A1 shows the coil support, including an inner copper current lead with a circular shape to ensure a robust solder joint between the superconducting tape and the current lead. The outer current lead is positioned sufficiently far from the coil to allow the attachment of the HTS tape at the end of the winding process.

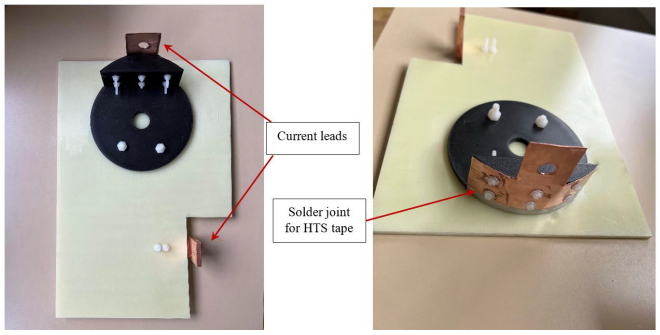

FIGURE A1. Support of the REBCO-based inductive coil and location of the current leads.

The electrical method is used for the characterization of the HTS coil. Fig. A2 illustrates the global experimental environment with the apparatus used for the DC and AC characterization of HTS.

Figure A3 illustrates the schematic of the experimental setup used for measuring the AC losses of HTS. The method involves measuring the current through the superconductor, the voltage across its terminals, and the phase difference between them. A sinusoidal current is supplied by an amplifier controlled by

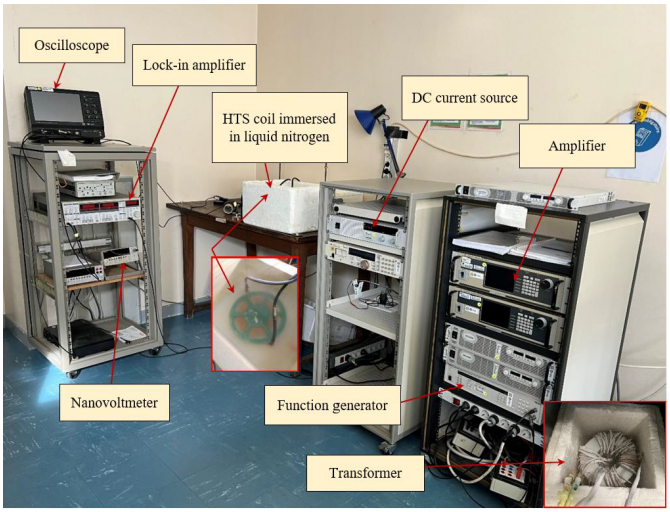

FIGURE A2. Experimental setup for the characterization of HTS. Measurement instruments are shown on the left, the power supplies on the right, and the studied HTS in the center.

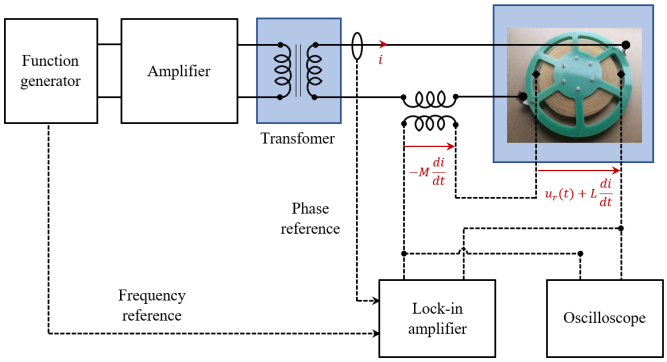

FIGURE A3. Schematic of the experimental setup for AC losses measurement in HTS.

a function generator, which sets the frequency and waveform. A transformer, immersed in liquid nitrogen, amplifies the current and provides galvanic isolation between the power and measurement sections. The waveform and root-mean-square (RMS) value of the supply current are measured using a Hall-effect probe at the secondary of the transformer, while the current and voltage across the superconductor are recorded with a lock-in amplifier and an oscilloscope.

The voltage across the HTS coil comprises a resistive component $u_r(t)$, representing the power losses, and an inductive component Ldi/dt, where L is the self-inductance of the HTS coil. Since the resistive component is much smaller than the inductive part, a compensation coil is connected in series with the voltage measuring circuit to partially or fully compensate the inductive part of the measured voltage. Its position and orientation are adjusted so that the mutual inductance M opposes the self-inductance L, improving the accuracy of the loss measurement.

REFERENCES

[1] Fukui, S., S. Tsukamoto, K. Nohara, J. Ogawa, T. Sato, and T. Nakamura, "Study on AC loss reduction in HTS coil for ar-

mature winding of AC rotating machines," *IEEE Transactions on Applied Superconductivity*, Vol. 26, No. 4, 1–5, Jun. 2016.

[2] Morandi, A., B. Gholizad, and M. Fabbri, "Design and performance of a 1 MW-5 s high temperature superconductor magnetic energy storage system," *Superconductor Science and Technology*, Vol. 29, No. 1, 015014, 2016.

[3] Song, W., X. Pei, J. Xi, B. Xiang, and Z. Liu, "Experimental AC loss analysis of braid type non-inductive coil for superconducting fault current limiter," *Journal of Physics: Conference Series*, Vol. 1559, No. 1, 012101, 2020.

[4] Li, Y., Z. Jiang, G. Sidorov, R. Koraua, Y. Sogabe, and N. Amemiya, "AC loss measurement in HTS coil windings coupled with iron core," *IEEE Transactions on Applied Superconductivity*, Vol. 29, No. 5, 1–5, 2019.

[5] Fawaz, S., H. Menana, B. Douine, and L. Queval, "Fast modeling approach of large-scale non-inductive HTS coils under different current supply," *Physica Scripta*, Vol. 98, No. 4, 045503, 2023.

[6] Mikitik, G. P., Y. Mawatari, A. T. S. Wan, and F. Sirois, "Analytical methods and formulas for modeling high temperature superconductors," *IEEE Transactions on Applied Superconductivity*, Vol. 23, No. 2, 8001920, 2013.

[7] Bean, C. P., "Magnetization of high-field superconductors," *Reviews of Modern Physics*, Vol. 36, No. 1, 31, 1964.

[8] Norris, W. T., "Calculation of hysteresis losses in hard superconductors carrying AC: Isolated conductors and edges of thin sheets," *Journal of Physics D: Applied Physics*, Vol. 3, No. 4, 489, 1970.

[9] Brambilla, R., F. Grilli, and L. Martini, "Development of an edge-element model for AC loss computation of high-temperature superconductors," *Superconductor Science and Technology*, Vol. 20, No. 1, 16–24, 2007.

[10] Zermeno, V. M. R., A. B. Abrahamsen, N. Mijatovic, B. B. Jensen, and M. P. Sørensen, "Calculation of alternating current losses in stacks and coils made of second generation high temperature superconducting tapes for large scale applications," *Journal of Applied Physsics*, Vol. 114, No. 17, 173901, 2013.

[11] Grilli, F., "Numerical modeling of HTS applications," *IEEE Transactions on Applied Superconductivity*, Vol. 26, No. 3, 1–8, 2016.

[12] Brandt, E. H., "Thin superconductors in a perpendicular magnetic ac field: General formulation and strip geometry," *Physical Review B*, Vol. 49, No. 13, 9024, 1994.

[13] Brandt, E. H., "Superconductors of finite thickness in a perpendicular magnetic field: Strips and slabs," *Physical Review B*, Vol. 54, No. 6, 4246, 1996.

[14] Statra, Y., H. Menana, L. Belguerras, and B. Douine, "A volume integral approach for the modelling and design of HTS coils," *COMPEL — The International Journal for Computation and Mathematics in Electrical and Electronic Engineering*, Vol. 38, No. 4, 1133–1140, 2019.

[15] Shanghai Superconductor Technology, "Second generation high temperature superconducting tape 2G-HTS Tapes," https://www.shsctec.com/products/tape (in Chinese).

[16] Kim, Y., C. F. Hempstead, and A. R. Strnad, "Magnetization and critical supercurrents," *Physical Review*, Vol. 129, No. 2, 528, 1963.

[17] Otten, S. and F. Grilli, "Simple and fast method for computing induced currents in superconductors using freely available solvers for ordinary differential equations," *IEEE Transactions on Applied Superconductivity*, Vol. 29, No. 8, 1–8, 2019.

[18] Fawaz, S., H. Menana, and B. Douine, "Numerical and experimental investigations of HTS coils inductance," *IEEE Transactions on Magnetics*, Vol. 58, No. 9, 1–4, 2022.

[19] Ekin, J., *Experimental Techniques for Low-temperature Measurements: Cryostat Design, Material Properties and Superconductor Critical-current Testing*, Oxford University Press, 2006.

[20] Fawaz, S., H. Menana, B. Douine, and L. Queval, "DC modeling and characterization of HTS coils with non uniform current density distribution," *Superconductor Science and Technology*, Vol. 34, No. 12, 124001, 2021.